Fused-Ring Systems

Deutsche Ausgabe: DOI: 10.1002/ange.201503553
Internationale Ausgabe: DOI: 10.1002/anie.201503553

Extended Corannulenes: Aromatic Bowl/Sheet Hybridization**

Amit K. Dutta, Anthony Linden, Laura Zoppi, Kim K. Baldridge, and Jay S. Siegel**

Abstract: *Among sheet/sheet polynuclear aromatic hydrocarbon (PAH) hybrids, a buckybowl–graphene hybrid has been used as a model to explore the effects of physical properties of PAHs with distinct planar and bowl regions. Activation of a C(Ar)−F bond was used to synthesize this corannulene/graphenic hybrid. Photophysical and voltammetric studies together with high-level computations revealed curvature and extended π-effects on the properties of these materials.*

Carbon π-system materials owe their multitude of properties to a diversity of allotropic topologies such as closed surfaces,[1] tubes,[2] and sheets.[3] Within the concept of sheet topology, conical (i.e. bowl)[4] and warped morphologies[5] complement classical planar graphenic forms. Curvature induces a shift in the orbital levels and HOMO–LUMO gap compared to a reference graphenic form.[6] Sheet topological materials with mixed planar and curved regions open the possibility for controlling the electronic properties and frontier orbital profile/pattern across the sheet. Specifically,

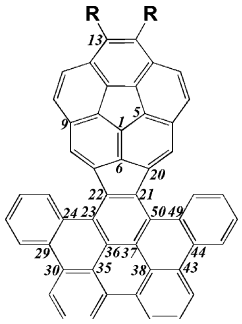

Scheme 1. Carbon atom numbering for **2**-R (R = H or Me).

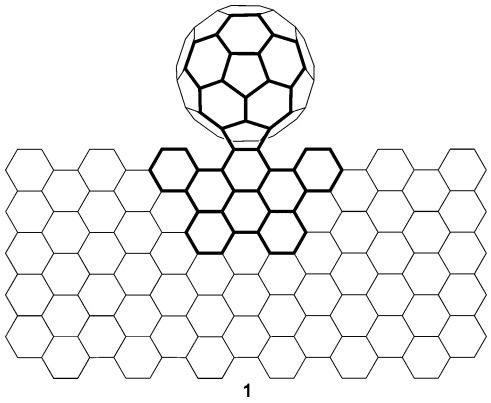

1

the buckybowl–graphene hybrid is an attractive family of synthetic targets.

The hypothetical graphene/fullerene nanobud[7] (**1**) exemplifies one kind of target that can be generated by conjugating a curved closed-surface with a planar sheet topology. Within the realm of bowl/sheet hybrids, corannulene/graphenic hybrid **2**-Me serves as a model to explore the effects of the physical properties of a PAH with distinct planar and bowl regions (Scheme 1).[8]

The synthesis of **2**-Me follows closely the previously reported synthesis of tetraarylindenocorannulenes,[9] with the addition of a silyl-cation-induced intramolecular Friedel–Crafts cycloarylation (Scheme 2).[10] Microwave-assisted, Pd-PEPPSI-IPent-mediated catalysis improves the arene–acetylene coupling to transform dichlorocorannulenedicarboxylate **3** into **4**.[11] The metal-mediated [2+2+2][12] reaction of **4** with tolan yields tetraarylindenocorannulene **5**, with fluorine-substituted arenes in positions 7 and 10.[13] Two-step reduction of the esters yields the corresponding dimethyl derivative (**7**).[14] Finally, a silyl-cation-induced intramolecular Friedel–Crafts arylation on **7** closes the flanking positions, and an

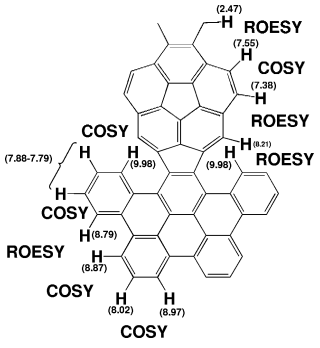

Figure 1. NMR spectroscopic assignments for **2**-Me deduced from COSY and ROESY data. Chemical shift values in ppm relative to CD_2Cl_2.

[*] Dr. A. K. Dutta,[+] Prof. Dr. A. Linden, Dr. L. Zoppi, Prof. Dr. K. K. Baldridge,[+] Prof. Dr. J. S. Siegel[+]
Department of Chemistry, University of Zurich
Winterthurerstrasse 190, 8057 Zurich (Switzerland)
E-mail: kimb@chem.uzh.ch

[+] Present address: School of Pharmaceutical Science and Technology
Tianjin University
92 Weijin Road, Nankai District, Tianjin-3000072 (China)
E-mail: dean_spst@tju.edu.cn

[**] K.K.B., J.S.S., and A.K.D. thank the National Basic Research Program of China (2015CB856500), the Qian Ren Scholar Program of China, and the Synergetic Innovation Center of Chemical Science and Engineering (Tianjin) for support of this work. L.Z. and K.K.B. thank the University of Zürich and URPP LightChEC program, as well as the CSCS supercomputing center for a grant of computer time. A.L. would like to thank the Swiss National Science Foundation for support of this work.

Supporting information for this article is available on the WWW under http://dx.doi.org/10.1002/anie.201503553.

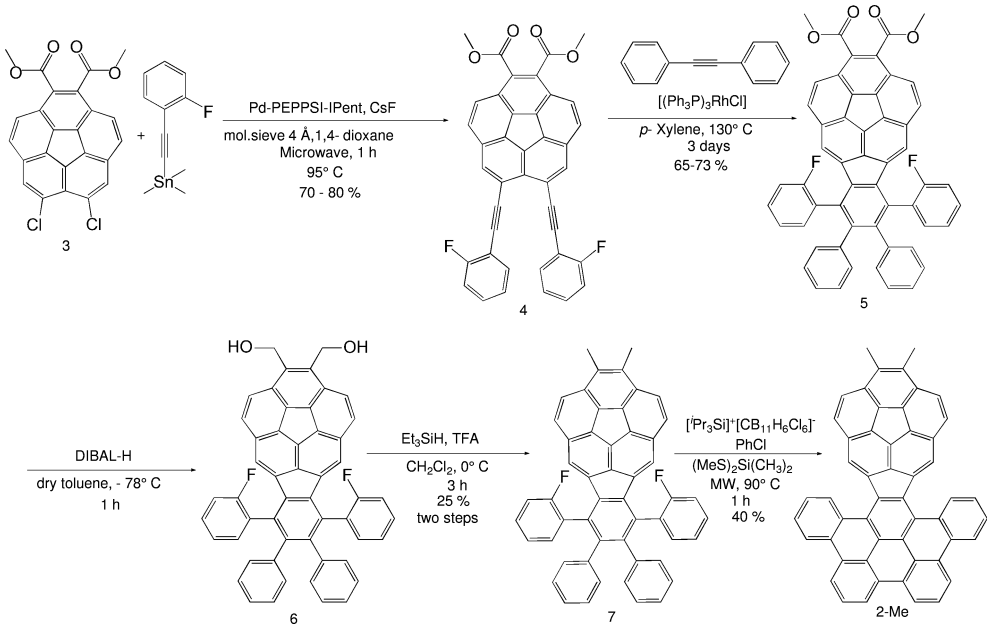

Scheme 2. Synthesis of buckybowl–graphene hybrid **2**-Me.

accompanying air oxidation/rearomatization completes the synthesis of **2**-Me.

Structure determination of **2**-Me proceeded from 2-D NMR studies in solution and X-ray crystallography. From the COSY and ROESY data (Figures S12–S14; Supporting Information) one can clearly assign the ^{1}H NMR spectrum of **2**-Me (Figure 1). The ROESY cross-peaks and differentiating chemical shifts support the idea of a sterically crowded border between the formal corannulene and graphene regions.

Dark orange crystals grown from dichloromethane diffract X-rays well (Figure 2); the structure derived reveals a triclinic unit cell (space group $P\bar{1}$) with two independent molecules of **2**-Me in the asymmetric unit together with accompanying solvent. The overall geometry, as gauged from bond lengths and angles, is in line with numerous reported corannulene structures (Table S1, Supporting Information).

The degree of "hinge" folding and bowl curvature are the most characteristic structural features of **2**-Me.[15] In the corannulene region, the bowl depth, as gauged from the hub atom to best rim plane, ranges from 1.02 to 1.15 Å, with an average of 1.07(4) Å; $POAV_{hub}$ angles[16] are 9.19°, 9.91°, and 10.91°. The graphenic region shows a bowing, but remains relatively close to its planar ideal with POAV angles $<1°$.[17] The average hinge angle, as defined by the dihedral angle of the best plane of the graphenic region (C23–C50) and bowl region (C1–C20), is 65.53(12)°; approximating the hinge angle on the basis of the best hub plane (C1–C5) and core benzene ring (C34–C39) gives a value of 60.93(12)°. B97D/Def2-TZVPP computations predict well the experimental geometry, including the bowl depth (1.106 Å) and hinge angle (graphenic and bowl planes: 70.2°//hub and core benzene planes: 65.7°) features. The bowl depth and POAV angles of the corannulene region agree within <0.04 Å and $<0.4°$, respectively. The predicted hinge angle deviates from that observed crystallographically by only about 5°.

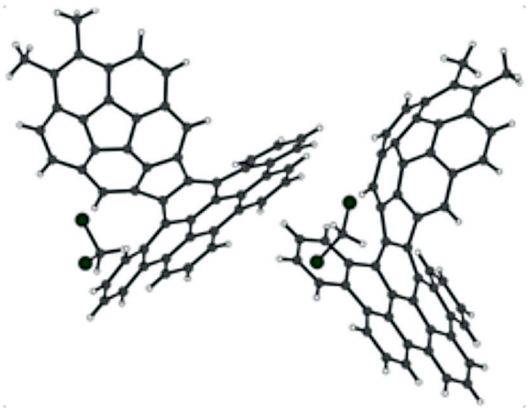

Figure 2. The asymmetric unit in the crystal structure of buckybowl–graphene hybrid **2**-Me + 2·CH_2Cl_2.

In **2**-R there are two large motion processes to consider: bowl inversion and hinge folding. Both motions independently relate two diastereomeric conformations **2′** and **2″** (Figure 3). The crystallographically observed conformer (cf. Figure 2) is predicted to be more stable than the alternative diastereomer by 8.2 kcal mol^{-1}, thus indicating that, independent of hinge folding dynamics, the population of the minor isomer is likely to be less than the detection limit of the NMR methods. In addition, as interconversion of these diastereomers does not create a dynamic symmetry, dynamic NMR line shape is not a useful technique to assess the hinge motion.

The steric character across the hinge can be likened to a *meso* pair of 5-helicenes (Figure 3). Depending upon the mechanism of hinge folding (concerted, $\mathbf{H}^2$, versus stepwise, **H** "helix" inversion) the barrier to hinge-isomer interconversion could range from 15 to 30 kcal mol^{-1}; bowl inversion, **B**, would also interconvert the diastereomers by an alternate mechanism, the barrier to interconversion by bowl inversion would be around 25–30 kcal mol^{-1}.[9]

The electronic structure model depicts the HOMO and LUMO of **2**-H extending well over the planar and bowl regions; however, the corannulene (bowl) region dominates the LUMO and the graphenic (planar) region dominates the HOMO, consistent with the idea that local curvature can be used to focus orbital and electron density in carbon sheets (Figure 4). The nucleophilic LUMO contour plot indicates a high probability that attack by nucleophiles will be at the edge of the bowl region, near the hinge of the structure.

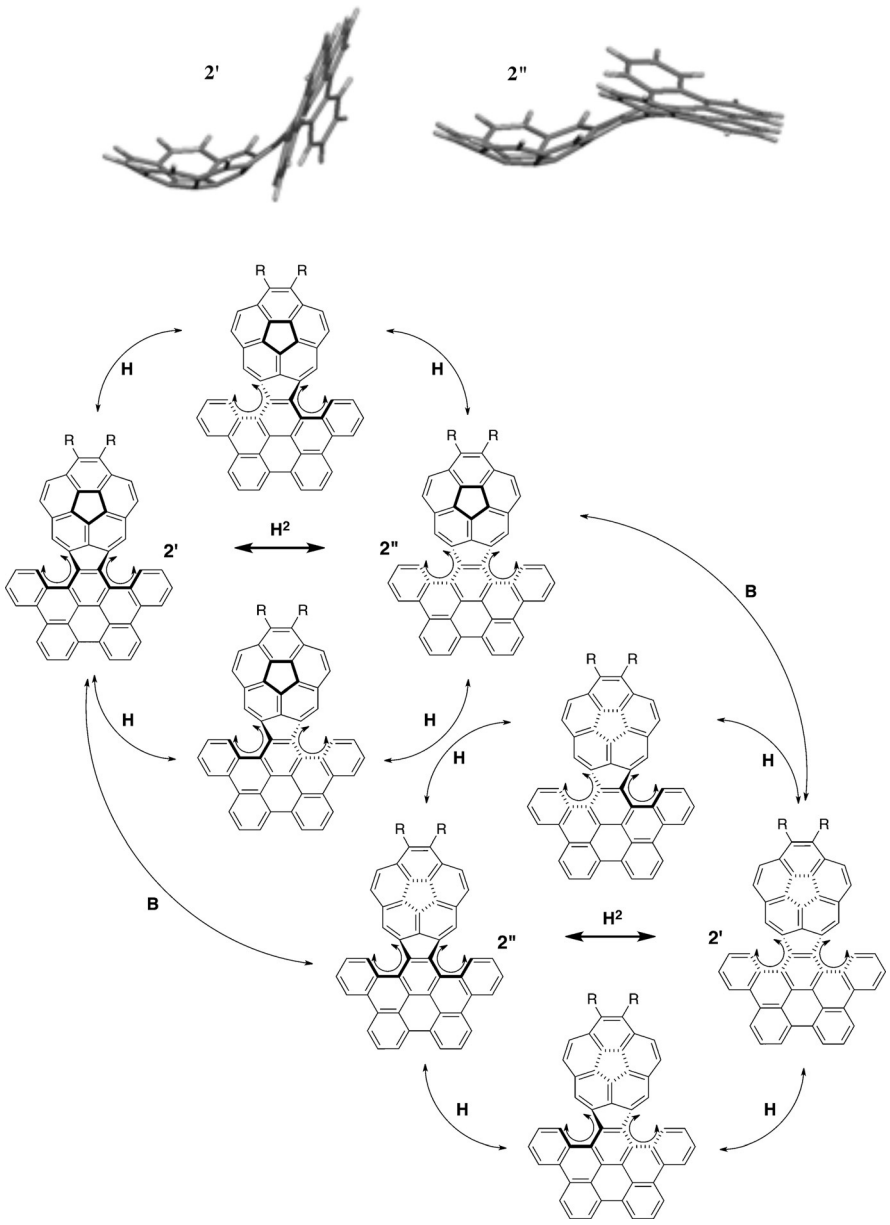

Figure 3. Conformations (**2′**/**2"**) and graph of diastereomer interconversion by helix (**H**) or bowl (**B**) inversion.

To place these features into a structural context, a series of reference compounds were considered for electrochemical and photophysical studies, including corannulene (**8**), benzo-hemicoronene (**9**), indenocorannulene (**10**), and **2**-Me (Figure 5). Using the first reduction potential as a gauge of electron affinity, the measured and B97D/Def2-TZVPP computed potentials were determined, and found to match very closely (Table 1). Optical band gaps determined from the onset of the absorption spectrum and GW-BSE-computed also agree well. Additionally, $GW_{HOMO-LUMO}$ gaps were calculated. This ensemble of electrochemical and photophysical data clearly indicates that the size and curvature of the π-systems play an important role in modulating reduction potential.

Motivated by the basic results, an extended series of compounds **11**–**14** was analyzed computationally to evaluate the effect of wrapping the bowl/sheet hybrid into a tube (Figure 6). The predicted first reduction potentials for **11** and **12** are 0.08 V and 0.05 V lower than those of **2′**-H, which is a direct consequence of their increased "box length" (**11**) and curvature (**12**) from that of **2′**-H, respectively. The effects, as gauged from the experimental or computed model series, reveal a crudely additive property (Figure 7), indicating one may be able to develop transferable parameters for "region types" in the design of morphology-dictated features of graphenic sheets. The fused hybrid **14**, with the largest π-conjugation and highest degree of pyramidalization, is predicted to be the most easily reduced among the hybrid series (calcd 1st reduction potential, −1.67 V).

For the subseries, **2′**-H, **11**–**14**, computational predictions suggest a progression from bowl to tube[18]

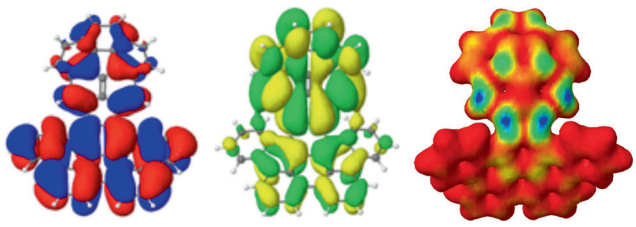

Figure 4. B97D/Def2-TZVPP calculated HOMO (left), LUMO (middle), and nucleophillic LUMO map (right; blue shows highest probability of attack by a nucleophile) of the major conformation of **2**-H.

Table 1: Reduction potential, $GW_{HOMO-LUMO}$, and optical gap for **8**, **9**, **10**, and **2**-R.

Compound	CV_{RedPot} [V] expt[a] (calcd)[b]	$GW_{HOMO-LUMO}$ gap	Optical gap expt (calcd GW-BSE)
8	−2.49 (−2.50)	7.2	3.5 (3.6)
9	−2.24 (−2.24)	5.6	2.8 (3.2)
10	−2.06 (−2.06)	6.0	3.1 (3.3)
2-Me (**2′**-H)	−1.87 (−1.88)	(5.7)	2.4 (2.5)

[a] Solvent: THF; working electrode: glassy carbon; reference electrode: Ag/Ag+ in acetonitrile; counter electrode: platinum wire; scan rate: 0.1 Vs^{-1}; supporting electrolyte: tetra-*n*-butylammonium hexafluorophosphate ($TBAPF_6$). [b] B97D/Def2-TZVPP: $E° = -\Delta G/nF + E_{ref}$, $n = 1$, $F = 1$ eV; $E_{ref} = -4.52$ [values referenced to Fc/Fc^+ in THF (+0.085 V)].

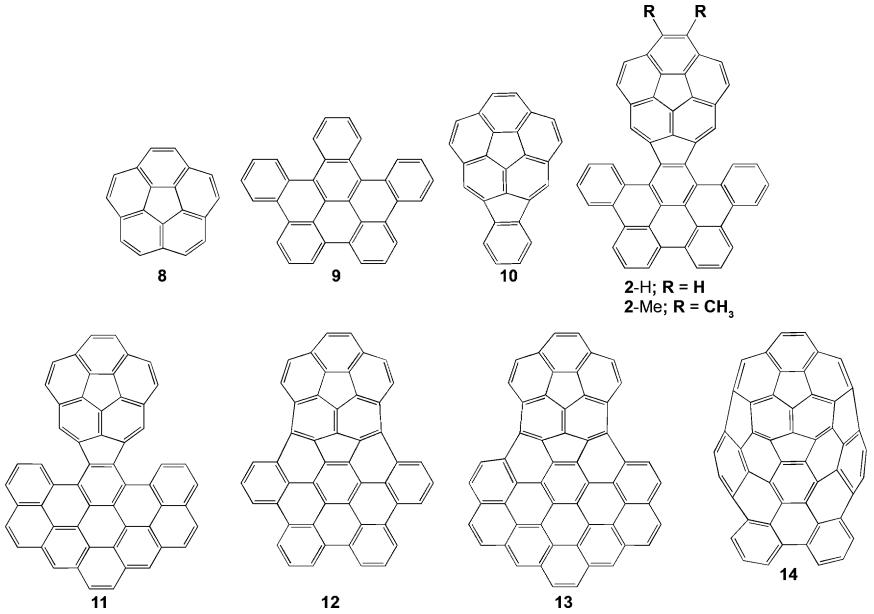

Figure 5. Compounds **2**-H/Me with reference set **8**–**14**.

Figure 6. B97D/Def2-TZVPP calculated structures of **2′**-H, **12** (fused), and **14** (tube) (from left to right) showing increasing surface curvature.

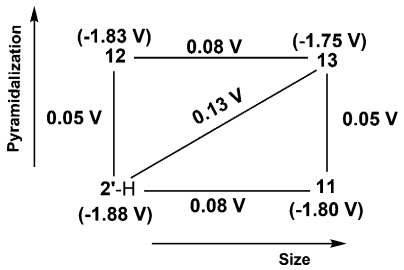

Figure 7. Comparative pyramidalization versus size relation based on B97D/Def2-TZVPP predicted reduction potentials of **2′**-H, **11**, **12**, and **13**.

Table 2: B97D/Def2-TZVPP-calculated electrochemical data and GW $gap_{HOMO-LUMO}$.

Property	**2′**-H	**11**	**12**	**13**	**14**
red_{CV}[V]	−1.88	−1.80	−1.83	−1.75	−1.67
$gap_{HOMO-LUMO}$	5.7	–	5.6	–	5.2
POAV angles	11.0, 7.3	10.9, 7.4	11.6, 11.1	11.5, 10.9	12.4, 12.7

(Figure 6). Calculated POAV values correlate well with the respective first reduction potential (Table 2), and indicate that pyramidalization to sp^2-hybridized carbon facilitates reduction.

The photophysical properties for **2**-Me as well as the reference series are reported in Table 3. Across the series, one sees an expected increase in the longest absorption wavelength as a function of system size and curvature (from 320 nm for the smallest system, **8**, to 494 nm for the largest system, **2**-Me). This trend maps directly with the predicted $GW_{HOMO-LUMO}$ gap values (Tables 1 and 2). Lifetimes across the series are 3–7 ns.

Somewhat unexpected is that the Stoke′s shift for **2**-Me is closer to that of the flat species **9** than to those of either the curved species **8** or **10**. This perhaps is indicative that the principal luminescent process occurs from state overlap in the flat region of **2**-Me avoiding the need for large structural rearrangement.

Table 3: Experimental photophysical properties in CH_2Cl_2 for **8**, **9**, **10**, and **2**-Me.

Property[a]	**8**	**9**	**10**	**2**-Me
λ_{abs} (log ε)	288 (4.7), 320 (4.0)	311 (4.8), 325 (4.8), 353(sh), 376(sh), 399 (4.36), 422 (4.4)	297 (4.3), 310 (4.4), 322(4.3), 338(4.3), 357-(sh), 374(3.7)	316 (4.4), 389 (4.4), 422 (4.1), 461 (3.0), 494 (3.5)
λ_{em}	420, 436	442, 460	556	509, 542
Stokes shift	1	5	0.55	6.7
λ_{excite}	318	325	340	397
QY(Φ_f)	1.63%	52.4%	0.7%	3.2%
τ (ns)	7.3	3.04	2.6	6.15

[a] abs = absorption (nm), em = emission (nm), Stokes shift = $\lambda_{em}-\lambda_{abs}$ ($\times 10^5$ cm^{-1}), excite = excitation (nm), τ = lifetime (ns).

Quantum yields reveal a morphological effect in which greater curvature leads to a reduced quantum yield.[19] This phenomenon could possibly be explained by a curvature-induced nonradiative internal conversion mechanism. Relative to the other curved members of the series (**8**, 1.63% and **10**, 0.7%), the quantum yield of **2**-Me appears to be somewhat enhanced by hybridization to the flat graphenic region. This effect may also indicate that the principal luminescent process occurs from state overlap in the flat region of **2**-Me.

Keywords: buckybowl–graphene hybrids · fused-ring systems · polyaromatic hydrocarbons · structure–activity relationships

How to cite: *Angew. Chem. Int. Ed.* **2015**, *54*, 10792–10796
Angew. Chem. **2015**, *127*, 10942–10946

[1] For comprehensive overviews, see for example: a) A. Hirsch, *Fullerenes and Related Structures*, Springer, Berlin, **1999**; b) A. Hirsch, M. Brettreich, *Fullerenes*, Wiley-VCH, New York, NY, **2005**.

[2] a) D. M. Guldi, N. Martin, *Carbon Nanotubes and Related Structures*: Synthesis Characterization, Functionalization, and Applications, Wiley-VCH, Weinheim, **2010**; b) M. S. Dresselhaus, G. Dresselhaus, P. Avouris, *Carbon Nanotubes: Synthesis Structure, Properties and Applications*, Springer, Berlin, **2001**.

[3] a) K. S. Novoselov, V. I. Fal′ko, L. Colombo, P. R. Gellert, M. G. Schwab, K. Kim, *Nature* **2012**, *490*, 192–200; b) K. K. Baldridge, J. S. Siegel, *Angew. Chem. Int. Ed.* **2013**, *52*, 5436–5438; *Angew. Chem.* **2013**, *125*, 5546–5548.

[4] First synthesis of corannulene: a) W. E. Barth, R. G. Lawton, *J. Am. Chem. Soc.* **1966**, *88*, 380–381; Reviews on geodesic polyarenes: b) Y.-T. Wu, J. S. Siegel, *Chem. Rev.* **2006**, *106*, 4843–4867; c) H. Hopf, *Classics in Hydrocarbon Chemistry*, Wiley-VCH, Weinheim, **2000**.

[5] a) T. J. Seiders, J. S. Siegel, *Chem. Br.* **1994**, *30*, 313–316; b) B. Kumar, R. L. Viboh, M. C. Bonifacio, W. B. Thompson, J. C. Buttrick, B. C. Westlake, M.-S. Kim, R. W. Zoellner, S. A. Varganov, P. Mçrschel, J. Teteruk, M. U. Schmidt, B. T. King, *Angew. Chem. Int. Ed.* **2012**, *51*, 12795–12800; *Angew. Chem.* **2012**, *124*, 12967–12972; c) C.-H. Feng, M.-W. Kuo, Y.-T. Wu, *Angew. Chem. Int. Ed.* **2013**, *52*, 7791–7794; *Angew. Chem.* **2013**, *125*, 7945–7948; d) K. Kawasumi, Q. Zhang, Y. Segawa, L. T. Scott, K. Itami, *Nat. Chem.* **2013**, *5*, 739–744.

[6] a) A. H. Castro Neto, F. Guinea, N. M. R. Peres, K. S. Novoselov, A. K. Geim, *Rev. Mod. Phys.* **2009**, *81*, 109–162; b) V. Kapko, D. A. Drabold, M. F. Thorpe, *Phys. Status Solidi B* **2010**, *247*, 1197–1200.

[7] The term "nanobud" was first coined for a fullerene–nanotube hybrid, see a) A. G. Nasibulin, P. V. Pikhitsa, H. Jiang, D. P. Brown, A. V. Krasheninnikov, A. S. Anisimov, P. Queipo, A. Moisala, D. Gonzalez, G. Lientschnig, A. Hassanien, S. D. Shandakov, G. Lolli, D. E. Resasco, M. Choi, D. Tománek, E. I. Kauppinen, *Nat. Nanotechnol.* **2007**, *2*, 156–161; for graphene nanobuds, see b) X. Wu, X. C. Zeng, *Nano Lett.* **2009**, *9*, 250–256; c) Y. Zheng, L. Xu, Z. Fan, N. Wei, Y. Lu, Z. Huang, *Curr. Nanosci.* **2012**, *8*, 89–96.

[8] An example of a bowl morphology in a mixed arene/alkane structure has been reported in the form of a tribenzotriquinane/graphene, see E. U. Mughal, D. Kuck, *Chem. Commun.* **2012**, *48*, 8880–8882.

[9] Y.-T. Wu, T. Hayama, K. K. Baldridge, A. Linden, J. S. Siegel, *J. Am. Chem. Soc.* **2006**, *128*, 6870–6884.

[10] O. Allemann, S. Duttwyler, P. Romanato, K. K. Baldridge, J. S. Siegel, *Science* **2011**, *332*, 574–577.

[11] M. Dowlut, D. Mallik, M. G. Organ, *Chem. Eur. J.* **2010**, *16*, 4279–4283.

[12] Alkyne trimerization with Wilkinson′s catalyst, see a) B. Witulski, C. Alayrac, *Angew. Chem. Int. Ed.* **2002**, *41*, 3281–3284; *Angew. Chem.* **2002**, *114*, 3415–3418; b) B. Witulski, T. Stengel, J. M. Fernandez-Hernandez, *Chem. Commun.* **2000**, 1965–1966; c) B. Witulski, T. Stengel, *Angew. Chem. Int. Ed.* **1999**, *38*, 2426–2430; *Angew. Chem.* **1999**, *111*, 2521–2524.

[13] Single isomers of either **5** or **7** can be separated chromatigraphically; however, a mixture of rotamers is apparent within minutes by NMR spectroscopy, thus suggesting a rotational barrier ca. 18 kcal mol^{-1}; see D. Gust, *J. Am. Chem. Soc.* **1977**, *99*, 6980–6982.

[14] a) F. A. Davis, D. L. Fanelli, *J. Org. Chem.* **1998**, *63*, 1981; b) B. D. Roth, C. J. Blankley, A. W. Chucholowski, E. Ferguson, M. L. Hoefle, D. F. Ortwine, R. S. Newton, C. S. Sekerke, D. R. Sliskovic, C. D. Stratton, M. W. Wilson, *J. Med. Chem.* **1991**, *34*, 357–366.

[15] The geometries reported herein are for symmetry-unique sites averaged over the two molecules in the asymmetric unit unless otherwise specified.

[16] POAV (p-orbital axis vector): a) R. C. Haddon, *Science* **1993**, *261*, 1545–1550; b) R. C. Haddon, *J. Am. Chem. Soc.* **1990**, *112*, 3385–3389; c) R. C. Haddon, *Acc. Chem. Res.* **1988**, *21*, 243–249; d) R. C. Haddon, L. T. Scott, *Pure Appl. Chem.* **1986**, *58*, 137–142.

[17] Carbon atoms C21 and C22, which define the hinge, have a POAV of 2.1°.

[18] K. K. Baldridge, J. S. Siegel, *Theor. Chem. Acc.* **1997**, *97*, 67–71.

[19] C_{60} ($\Phi_f = 0.033\,\%$) has a lower quantum yield than that of the relatively less curved C_{70} ($\Phi_f = 0.054\,\%$), see B. Ma, Y.-P. Sun, *J. Chem. Soc. Perkin Trans. 2* **1996**, 2157–2162.

Received: April 19, 2015
Revised: June 25, 2015
Published online: July 24, 2015

